

Influence of the rippling on the collisionless ion and electron motion in the shock front: A model study

M. Gedalin

Department of Physics, Ben-Gurion University, Beer-Sheva, Israel

1. Introduction

The only well-developed theory of collisionless shocks is the one-dimensional (1-D) stationary theory, which explicitly assumes that all variables in the shock front, including electric and magnetic fields, depend only on the coordinate along the shock normal and do not depend on time. These two assumptions are essential for establishing the Rankine-Hugoniot relations [see, e.g., *Tidman and Krall*, 1971] which connect the upstream and downstream states of plasma and magnetic field, when these relations are intended to be applied to real shocks with nonzero thickness throughout the shock front. Moreover, our present understanding of the microscopic processes with ions and electrons at the shock front is based on the same assumptions of one-dimensionality and stationarity. All theoretical descriptions of the ion reflection and gyration [*Woods*, 1969, 1971; *Leroy et al.*, 1982; *Leroy*, 1983; *Lee et al.*, 1986; *Burgess et al.*, 1989; *Gedalin*, 1996a] assume that the shock is planar. A number of simulations have taken into account the shock curvature, mainly for studies of the high-energy ion acceleration [see, e.g., *Decker*, 1990], global bow shock geometry (foreshock formation and position) [*Thomas and Winske*, 1990; *Savoini and Lemege*, 1999], or nonlocal effects in the particle motion [*Krauss-Varban and Burgess*, 1991; *Vandas*, 1995a, 1995b]. Spatial inhomogeneity of the shock behind the shock front, in the form of magnetic loops [*Decker*, 1993], was also analyzed in the context of the shock drift acceleration theory.

However, all theoretical developments concerning local structure of the shock front are still done in the one-dimensional stationary model. All derivations of the foot length [*Woods*, 1969, 1971; *Livesey et al.*, 1984; *Gosling and Robson*, 1985; *Gosling and Thomsen*, 1985] are done with the assumption that the shock is strictly one-dimensional, at a scale down to the ion convective gyroradius. All theoretical descriptions of the electron heating by the cross-shock electric potential, including various Liouville mappings of upstream-to-downstream distribution [*Feldman et al.*, 1982; *Goodrich and Scudder*, 1984; *Feldman*, 1985; *Schwartz et al.*, 1988; *Wilkinson and Schwartz*, 1990; *Balikhin et al.*, 1993; *Gedalin et al.*, 1995a, 1995b; *Scudder*, 1995; *Ball and Galloway*, 1998; *Hull et al.*, 1998], do not take into account possible deviations from the one-dimensional stationary structure, yet two- and three-dimensional hybrid simulations [*Winske and Quest*, 1988; *McKean et al.*, 1995; *Hellinger and Mangeney*, 1997] show that the shock front is, most probably, three-dimensional (rippled). This rippling is usually attributed to the shock nonstationarity, that is, wave crossing of the shock front. Oblique ion-cyclotron waves (peak power at $\theta_{Bk} \approx 60^\circ$ is found by *McKean et al.* [1995]) are considered to be the most plausible candidates for the role of these waves, yet there is no explanation for how these waves could have already grown to such high amplitudes (comparable to the overall magnetic field jump) at the upstream side of the ramp (which is necessary to cause noticeable rippling) or how these waves (wavelengths of the order of several ion inertial lengths at least [*McKean et al.*, 1995]) cannot exist inside a ramp whose width typically does not exceed one ion inertial length [*Newbury et al.*, 1998]. Thus it is possible that this rippling is not a result of any instability and wave growth but is an inevitable part of the shock structure (see below) and a manifestation of the intrinsic shock dynamics (probably, in the spirit of *Krasnosel'skikh* [1985], if it is nonstationary). It is worth mentioning that such rippling was found to occur in the direction of the magnetic field [*McKean et al.*, 1995] as well as in the perpendicular direction [*Savoini and Lemege*, 1994] (the last one was observed in two-dimensional full particle simulations). There is also limited observational evidence in favor of the shock rippling based on the fact that the locally found shock normal direction varies substantially across the shock front and often differs for two spacecraft-measured profiles. It is impossible to conclude whether such rippling is related to nonstationary phenomena, at least before the Cluster mission. Numerical simulations have their own limitations and do not allow unambiguous conclusions either.

During their motion in the shock, ions and electrons move along the shock front by a distance of the order of ion inertial length c/ω_{pi} or even greater, and if the shock front is inhomogeneous at these scales, that may well affect the particle motion, even if nonstationary features are absent from or weak in the near-ramp vicinity. In this case the ion motion may appear to be strongly coupled to the shock rippling phenomenon.

Recently, *Gedalin et al.* [2000] analyzed ion motion in an observed high Mach number shock. The shock was found to be stationary according to the two-spacecraft measurements. However, analyzing the ion motion in this shock front, *Gedalin et al.* [2000] have shown that the observed shock parameters and the shock's apparent stability are inconsistent with the assumption that the shock is one-dimensional and stationary: variations of the downstream ion pressure are too high to ensure the pressure balance across the shock. If the shock is not one-dimensional and stationary, it may be spatially inhomogeneous along the shock front (rippled), nonstationary at the typical ion timescale $1/\Omega_i$, or both. Since some high Mach number shocks look pretty stationary when viewed by two spacecraft, we have to study the effects of rippling alone.

Therefore one has to study deviations from this simple one-dimensional stationary structure to improve our understanding of the collisionless shock physics. The objective of the present paper is to study ion and electron motion in the rippled (spatially inhomogeneous along the shock front) shock. *Winske and Quest* [1988] and *McKean et al.* [1995] suggested that the shock rippling is caused by Alfvén-ion-cyclotron waves (AIC) excited in the shock front with wave vectors in the coplanarity plane (not necessarily along the magnetic field). *Hellinger and Mangeney* [1997] suggest that rippling appears only in sufficiently high Mach number shocks, where AIC have enough time to grow in the shock front. Recently, *Gedalin et al.* [2000] proposed another explanation of the rippling, related to the impossibility of establishing pressure balance in one-dimensional high Mach number shocks. We would like to know whether such rippling can make the downstream ion distribution more smooth and diffuse to reduce the fluctuations of the plasma parameters, so that the shock stability may be improved. (*Hellinger and Mangeney* [1997] suggest that rippling may reduce the downstream ion temperature anisotropy.) Analysis of a one-dimensional shock has shown [*Gedalin et al.*, 2000] that the ion distribution just behind the ramp gyrates as a whole. This gyration is too coherent in the sense that all ions essentially turn around at the same place, which results in strong ion bunching and excess of the ion kinetic pressure near the turning points. It was suggested, on the basis of two-dimensional hybrid simulations [see, e.g., *McKean et al.*, 1995] that waves are excited by the nongyrotropic ion distribution behind the ramp, and it is these waves which rapidly smooth the downstream ion distribution via wave-particle interaction. It is, however, unclear how this wave-particle interaction can be efficient at the scale of one ion gyroradius (necessary to reduce the ion pressure peaks, which are responsible for breakdown of pressure balance condition). Standard description of the turbulent wave-particle interaction with, e.g., ion-cyclotron waves, requires participation of a large number of waves with stochastically distributed phases with gyrating ions, and the interaction time should be much larger than the ion gyroperiod. In this case, however, the interaction occurs in a strongly nonlinear, strongly inhomogeneous region on a part of the ion gyrotrajectory, so that the wave-ion coupling can be quite different. It is possible that the magnetic field fluctuations are directly related to the currents produced by the bunching of gyrating ions and not by instabilities. Moreover, the presented ion distributions are averaged in the direction of rippling [*McKean et al.*, 1995], so that nonlocal effects are mixed with the local interactions.

Electrons may be affected by the shock rippling too, since they drift along the shock front by a distance comparable to the ion inertial length, and if the conditions change along the shock front, different electrons may well cross different cross-shock potentials, acquiring different energies. Collisionless models [*Goodrich and Scudder*, 1984; *Schwartz et al.*, 1988; *Wilkinson and Schwartz*, 1990; *Balikhin et al.*, 1993; *Gedalin et al.*, 1995a, 1995b; *Scudder*, 1995; *Ball and Galloway*, 1998; *Hull et al.*, 1998; *Gedalin and Griv*, 1999] predict the formation of large holes in the electron distribution which begins to form in the ramp. Observations [*Feldman et al.*, 1982; *Feldman*, 1985] show flattop distributions instead of such holes (see, however, *Bale et al.* [1998]). Existing numerical simulations of electrons in the shock front try to reproduce the observed distributions by either introducing effective collisions via the Monte Carlo method [*Veltri et al.*, 1990, 1992; *Veltri and Zimbardo*, 1993a, 1993b] or taking into account collisional effects self-consistently [*Lembege and Savoini*, 1992; *Savoini and Lembege*, 1994; *Krauss-Varban et al.*, 1995] and averaging along the shock front, thus losing information about the local effects of macroscopic fields and distribution formation. It is still not clear whether the electron motion in the shock front is essentially collisionless or effective collisions play an important role in the formation of the electron distribution function while the energetics is determined by the cross-shock potential. Shock rippling could substantially affect the shape of the collisionlessly formed holes in electron distributions.

It therefore makes sense to study the effects of stationary but rippled fields on the ion and electron motion, leaving aside wave-particle interactions, to achieve better understanding of the shock physics, in particular, of whether macroscopic quasistationary fields may be responsible for the prompt ion distribution smoothing. Our approach is quite straightforward. We choose a shock model (electric and magnetic fields) and numerically trace ions and electrons across this structure. The information sought for is deduced from the particle trajectories. We leave aside all nonstationarity to study the effects of spatial inhomogeneity alone. We emphasize the difference of our approach from self-consistent numerical simulations. The latter inevitably take into account everything, including macroscopic field, instabilities, and wave-particle interactions. On the other hand, our goal is to isolate specific physical effect related to the spatial inhomogeneity, which might occur even when the shock front is stationary and in the absence of turbulence. The objective is to compare the particle dynamics in the one-dimensional structure with the particle dynamics in the rippled structure and not with the particle features in observed shocks (which is impossible with the presently available data and in the absence of reliable observational separation of temporal and spatial variations), so that usage of a model shock profile instead of an observed one is almost mandatory.

The paper is organized as follows. Section 2 describes the choice of the shock model. In section 3 we present the results of the analysis of the ion motion. Electron motion is described in section 4. The implications of the numerical analysis are given in section 5.

2. Shock Model

Analytical study of the particle motion in a strongly inhomogeneous shock front does not seem to be possible, so in the present paper we shall use a model shock profile to numerically trace ion and electron trajectories.

Although observed high Mach number shocks usually possess well-defined small-scale structure [Newbury *et al.*, 1998], we shall use a rather simple monotonic magnetic field profile, bearing in mind that the main objective is to reveal major differences between particle motion in a one-dimensional structure and particle motion in a rippled shock. In doing that we will establish semiquantitatively the dependence of the effects on the rippling parameters.

In what follows, the coordinate x is along the shock normal of what would be the shock normal if the shock were one-dimensional. Coordinate y is along the noncoplanarity direction, while z is along the main magnetic field. The main magnetic field component is chosen in the following monotonic form:

$$B_z = \frac{B_{zu} + B_{zd}}{2} + \frac{B_{zd} - B_{zu}}{2} \tanh(X + X^3), \quad (1)$$

$$X = \left[x + a_y \sin\left(\frac{2\pi y}{L_y}\right) + a_z \sin\left(\frac{2\pi z}{L_z}\right) \right] / D, \quad (2)$$

where D is the ramp half width. The choice of the tanh argument ensures that the magnetic field B_z variations are confined inside the region $-1 < X < 1$. The choice of the argument X allows complete control over the rippling; a_y and a_z are the amplitudes and L_y and L_z are the spatial scales of the rippling in the y and z directions, respectively. Such sinusoidal rippling with small rippling amplitude and large $L_{y,z}$ (much greater than the ion convective gyroradius) was considered by Decker [1990] for high-energy ion acceleration in nearly perpendicular shocks. Here we are interested in the effects of the smaller-scale rippling on incident ions of the solar wind. In what follows, we shall assume that the rippling scale is of the order of the upstream ion convective gyroradius, while the rippling amplitude is less than the ion inertial length, which is the basic scale of the ramp [Newbury *et al.*, 1998]. This choice of parameters is determined by the observation that some high Mach number shocks seem stationary when measured by two spacecraft with spatial separation of several ion inertial lengths both along the shock normal and along the shock front [Newbury *et al.*, 1998; Gedalin *et al.*, 2000].

The noncoplanar magnetic field B_y is chosen as follows [cf. Jones and Ellison, 1987, 1991; Gedalin, 1996b]:

$$B_y = s_y (dB_z/dx), \quad (3)$$

where the coefficient s_y is introduced in order to make B_y resemble observations.

The normal component of the magnetic field B_x is obtained from the zero divergence condition $\nabla \cdot \mathbf{B} = 0$ in the following form:

$$\begin{aligned} B_x = B_{xu} - \frac{2\pi a_z}{L_z} (B_z - B_{zu}) \cos\left(\frac{2\pi z}{L_z}\right) \\ - \frac{2\pi a_y}{L_y} B_y \cos\left(\frac{2\pi y}{L_y}\right) \end{aligned} \quad (4)$$

and is no longer constant throughout the shock front. The upstream magnetic field components B_{zu} and B_{xu} can be expressed as $B_{xu} = B_u \cos \theta$, and $B_{zu} = B_u \sin \theta$, where B_u is the total upstream magnetic field and θ is the angle between the upstream magnetic field and the shock normal.

Stationarity of the shock implies potential character of the electric field, and we choose the cross-shock potential as follows [cf. Hull *et al.*, 1998; Gedalin and Griv, 1999; Gedalin *et al.*, 2000]:

$$\phi = s_e (B_z - B_{zu}), \quad (5)$$

where the coefficient s_e controls the overall cross-shock potential drop.

Expressions (1)-(4) for the model fields look somewhat arbitrary. It should be mentioned, however, that they are chosen to resemble more or less the observed fields, and in any case, the true examination should be done by comparison of the particle motion in the one-dimensional stationary structure with the particle motion in the rippled shock.

In what follows, we shall consider two cases of rippling: (1) rippling in the y direction ($a_z = 0$) and (2) rippling in the z direction ($a_y = 0$). Although theoretically nothing limits the possible direction of rippling, the above cases cover the possible physical effects in the presence of the periodic inhomogeneity of the shock surface.

For the present numerical analysis we chose the following shock parameters, similar to the parameters of the observed shock studied by Gedalin *et al.* [2000]: Mach number $M = 3.7$, magnetic compression $B_d/B_u = 3.5$, the angle between the shock normal and the upstream magnetic field is $\theta = 65^\circ$, and the ion and electron upstream pressures are described by $\beta_i = 0.05$ and $\beta_e = 0.15$. Thus the shock is a slightly supercritical (or marginally critical), quasiperpendicular, low- β shock. The ramp width $D \approx 0.3(c/\omega_{pi})$ is chosen to be of the order of but smaller than the ion inertial length, which is in agreement with observations [Newbury *et al.*, 1998]. In what follows, we measure all spatial scales in the upstream ion convective gyroradii V_y/Ω_u and ion inertial lengths c/ω_{pi} . Velocities are measured in the units of the upstream incident plasma velocity V_u (in the normal incidence frame).

Figure 1 shows the magnetic field components for the case of rippling in the y direction. The rippling scale is $L_y = 0.5(V_u/\Omega_u)$, while the rippling amplitude is $a_y = 0.3(c/\omega_{pi})$. The top panel shows the main magnetic field component. It

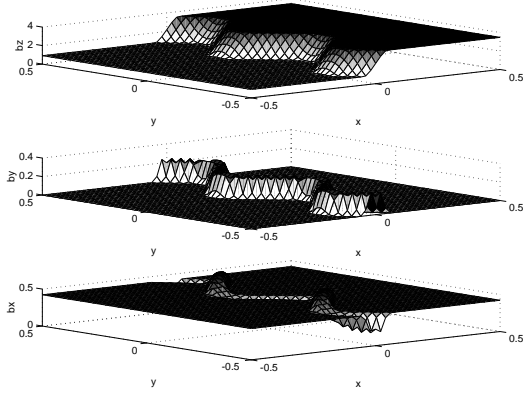


Figure 1. Three components of the magnetic field (from top to bottom: B_z , B_y , and B_x) for the case of the shock front rippled in the y -direction. The rippling scale $L_y = 0.5(V_u/\Omega_u)$, rippling amplitude $a_y = 0.3(c/\omega_{pi})$

is seen that as a result of the rippling the position of the magnetic field transition periodically depends on the coordinate y along the shock front. The middle panel shows the noncoplanar magnetic field component, which has a strong peak inside the ramp with the position of the peak following the (periodically dependent on y) position of the magnetic field transition. The bottom panel shows the normal component of the magnetic field. This field would be strictly constant throughout the shock front if the shock were one-dimensional. In the presence of the spatial inhomogeneity along the shock front this field component is no longer constant but spatially variable.

Figure 2 shows the model electric field (normalized on the upstream electric field) for the same case of the rippling in

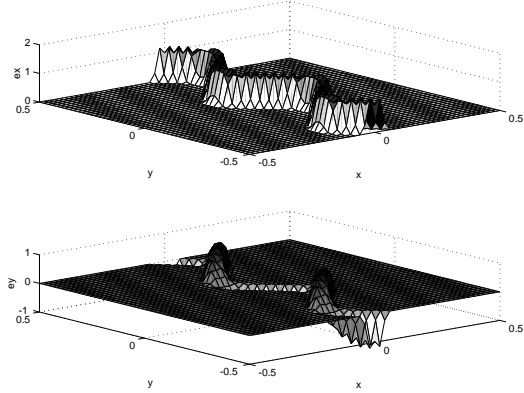


Figure 2. The components of the electric field ((top) E_x and (bottom) E_y), shown in the de Hoffman-Teller frame for the case of the shock front rippled in the y -direction. The rippling scale $L_y = 0.5(V_u/\Omega_u)$; rippling amplitude $a_y = 0.3(c/\omega_{pi})$. The electric field is normalized on the upstream NIF electric field $E_0 = V_u B_u \sin \theta / c$. E_z , the third component of the electric field, is identically zero throughout the shock.

the y -direction. The top panel shows the x component of the electric field, that is, the cross-shock electric field, which accelerates electrons across the shock and decelerates ions. It has a strong peak inside the ramp with the position following the position of the magnetic field transition. The bottom panel shows the motional component E_y of the electric field. We are working in the de Hoffman-Teller frame, and this field component would be zero throughout the shock if the shock were one-dimensional. Because of the periodic inhomogeneity along the shock front E_y becomes nonzero and spatially variable. However, the overall cross-shock potential remains independent of the coordinate along the shock front, so each particle crossing the shock would see the same potential drop. The third component of the electric field, E_z , vanishes throughout the shock.

Figure 3 shows the magnetic field for the case of rippling in the z direction. The rippling scale and amplitude are the same as in the previous case. The only difference with the y -rippling case is that the normal component of the magnetic field, B_x , now does not tend to any constant value downstream but remains periodically dependent on z . If an observer crossed the shock strictly along the shock normal (x direction), he would see this magnetic field component changing across

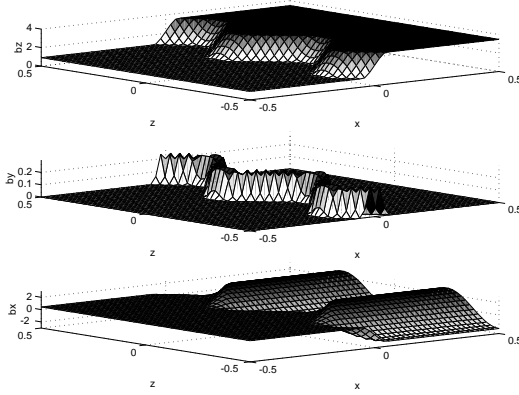


Figure 3. Three components of the magnetic field (from top to bottom: B_z , B_y , and B_x) for the case of the shock front rippled in the z -direction. The rippling scale $L_z = 0.5(V_u/\Omega_u)$; rippling amplitude $a_z = 0.3(c/\omega_{pi})$.

the shock. If an observer crossed the shock at an angle to the normal he would see this magnetic field changing periodically in time (in the observer's frame), so that the average normal magnetic field component remains unchanged across the shock front. It is difficult to assess whether such a situation realizes in nature on the basis of available observations or numerical simulations, since in all of them all magnetic field components strongly fluctuate just beyond the ramp of a high Mach number collisionless shock.

Figure 4 shows the electric field for the same shock rippled in the z direction. Now $E_y = 0$ throughout the shock front,

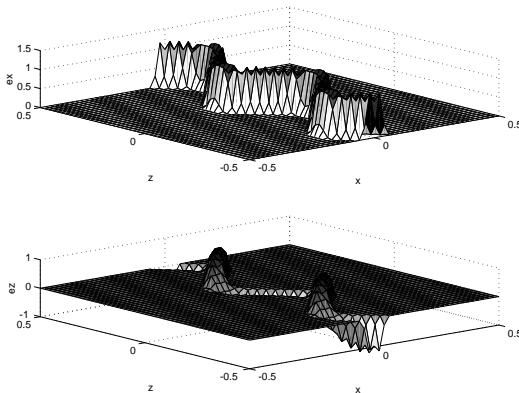


Figure 4. The electric field ((top) E_x and (bottom) E_z) shown in the de Hoffman-Teller frame for the case of the shock rippled in the z -direction. The rippling scale $L_z = 0.5(V_u/\Omega_u)$; rippling amplitude $a_y = 0.3(c/\omega_{pi})$. The third electric field component $E_y = 0$ throughout the shock.

while E_z is nonzero and spatially dependent. The most important difference with the previous case is that the relative velocity of the normal incidence (NIF) and de Hoffman-Teller (HT) frames is along the z direction, because of which the pattern that is stationary in one frame is time dependent in the other. That means that one has to consider at least two cases: when the rippled structure is stationary in the de Hoffman-Teller frame and when it is stationary in the normal incidence frame.

3. Ions

Once the rippled shock structure is established, we numerically trace charged particles in the stationary (but not one-dimensional) electric and magnetic fields of the shock. We start analysis with the ion motion. Ions are distributed Maxwellian initially far upstream of the shock front, where the fields are still homogeneous. Figure 5 shows the results of the tracing of 20 ions across the shock rippled in the y direction. For the presentation we have chosen the ion trajectory in the x - y plane. This plane is essentially perpendicular to the magnetic field, and this is the plane where the ion gyration occurs. The top panel corresponds to the one-dimensional structure ($a_y = 0$). For others the rippling scale $L_y = 0.5(V_u/\Omega_u)$ is the same, but the rippling amplitude a_y increases from top to bottom. It is easily seen that substantial rippling results in

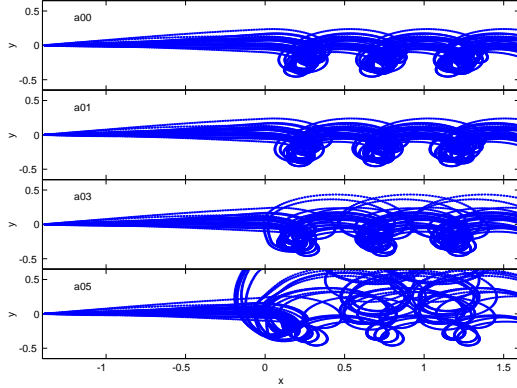


Figure 5. Trajectories of 20 ions with rippling in the y -direction. The rippling scale $L_y = 0.5(V_u/\Omega_u)$; the rippling amplitude $a_y = 0$ (no rippling), $0.1(c/\omega_{pi})$, $0.3(c/\omega_{pi})$, and $0.5(c/\omega_{pi})$ increases from top to bottom.

the significant scattering of ions. In the one-dimensional case all ions stop and turn essentially in the same point. Along with the effective broadening of the ion distribution, there is strong bunching of the ions near the turning point, which results in a substantial density increase and therefore peaks of the ion pressure. It is this bunching that is responsible for too high ion pressure peaks and breakdown of the pressure balance condition $nm_iV_x^2 + p_{e,xx} + p_{i,xx} + \mathbf{B}^2/2\mu_0 = \text{const}$ [Gedalin *et al.*, 2000]. However, if the rippling is substantial, different ions turn in different points, which makes the downstream ion distribution much more smooth and diffuse, thus reducing the variations of the downstream ion pressure, which is expected to improve the shock stability.

Figure 6 shows the trajectories of ions starting at different positions along the shock front. The top panel is for the one-

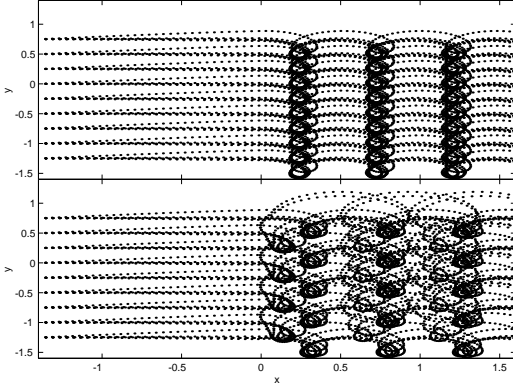


Figure 6. Trajectories of ions starting at the same initial x but different initial y positions. The top panel corresponds to the strictly one-dimensional case. For the bottom panel the shock is rippled in the y direction with the rippling scale of $L_y = 0.5(V_u/\Omega_u)$ and rippling amplitude $a_y = 0.3(c/\omega_{pi})$.

dimensional shock. The downstream pattern is strictly periodic, and there is strong bunching of ions near the turning point. The bottom panel is for moderate rippling. The ion distribution is much more diffuse. The ion reflection also becomes y dependent: whether an ion is reflected or not depends now not only on the ion initial velocity but also on its initial position along the shock front. The distribution of reflected ions also becomes more diffuse than in the one-dimensional case, which also works toward improving the shock stability.

In order to demonstrate the smoothing more quantitatively, we present in Figure 7 the hydrodynamical variables (density n , pressure p_{xx} , and temperature $T_{xx} = p_{xx}/n$) found numerically from the trajectory tracing throughout the shock front. The variables were obtained using the staying-time method [Gedalin *et al.*, 1995b] and averaging over the spatial period of inhomogeneity L_y . This averaging helps to reduce the effects of discreetness (this difficulty does not arise in the one-dimensional case but severely restricts us technically in the analysis of the rippled shock front). More important is the two-dimensional nature of the shock structure and ion distribution, while our numerical method of the determination of the moments of the distribution function is essentially one-dimensional and cannot be directly applied to the analysis of the two-dimensional geometry, and we have to invoke averaging along the shock front. Indeed, the particle number conservation

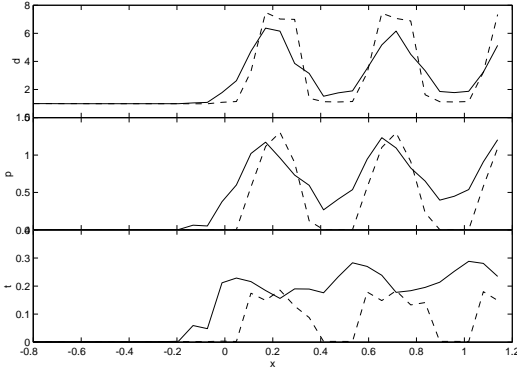


Figure 7. Comparison of ion hydrodynamical variables (density n in the top panel, pressure component p_{xx} in the middle panel, and temperature component $T_{xx} = p_{xx}/n$ in the bottom panel) for the case of strictly one-dimensional shock geometry (dashed lines) and the shock rippled in the y direction with the rippling scale of $L_y = 0.5(V_u/\Omega_u)$ and rippling amplitude $a_y = 0.3(c/\omega_{pi})$ (solid lines).

reads (stationary case)

$$\nabla_x(nV_x) + \nabla_i(vV_i) = 0, \quad (6)$$

where i stands for y and z and summation over i is implied. Assuming periodicity along y and z with the spatial periods L_y and L_z , respectively, and integrating (6), one immediately finds

$$\frac{d}{dx} \int_0^{L_y} dy \int_0^{L_z} dz n V_x = 0. \quad (7)$$

Similarly, momentum conservation can be written as follows:

$$\begin{aligned} & \nabla_x(nmV_x^2 + p_{xx}) + \nabla_i(nV_x V_i + p_{xi}) \\ &= \frac{1}{4\pi} (B_x \nabla_x + B_i \nabla_i) B_x - \frac{1}{8\pi} \nabla_x B^2. \end{aligned} \quad (8)$$

Using the relations $B_i \nabla_i B_x = \nabla_i(B_i B_x) - B_x \nabla_i B_i$ and $\nabla_i B_i = -\nabla_x B_x$, after integration one easily finds

$$\frac{d}{dx} \int_0^{L_y} dy \int_0^{L_z} dz (nmV_x^2 + p_{xx} + \frac{B^2 - 2B_x^2}{8\pi}) = 0. \quad (9)$$

Relations (7) and (9) are the generalization (with necessary averaging) of the continuity and pressure balance conditions onto the rippled shock case.

The hydrodynamical variables presented in Figure 7 are calculated using the above averaging. Figure 7 shows that the fluctuations of the hydrodynamical variables (including pressure) are substantially lower in the rippled shock case, which supports our (visually based) expectations of the distribution smoothing. The difference, though, is not especially strong. This is because the chosen shock parameters apparently allow quite good one-dimensional structure, and improvements are not crucial. It does not seem possible at this stage to perform testing of the rippling influence on a high-Mach shock stability, since our understanding of the structure of such shock is far from being perfect, yet earlier studies [Zilbersher *et al.*, 1998; Gedalin *et al.*, 2000] have shown that there should be fine tuning in shock parameters in order to ensure its very existence (and, moreover, its stationarity). Although the parameters used resemble the observed shock parameters [Gedalin *et al.*, 2000], the model field structure may lack important details necessary for a reliable analysis.

We can, however, try a shock profile where one-dimensional description is expected (or is known from other sources) to be not quite satisfactory. Figure 8 shows the comparison of the ion behavior for the shock with the parameters similar to those of the shock described by Gedalin *et al.* [2000] (it was shown that this shock is not one-dimensional): $M = 3.3$, $B_d/B_u = 2.8$, $\theta = 58^\circ$, $\beta_i = 0.05$, and $D = 0.1(c/\omega_{pi})$. This shock profile includes overshoot also, which is modeled by a Gaussian $\delta B_z = B_{\text{add}} \exp[-(X - X_o)^2/2D_0^2]$ (with suitably chosen parameters B_{add} , X_o , and D_o), superimposed on the profile described by (1).

For this presentation we have chosen the total (ram and kinetic) pressure $nm_i V_x^2 + p_{xx}$ and density. The pressure and density are averaged along y as prescribed by (7) and (9). The bottom panel shows the magnetic field which is calculated from the generalized pressure balance (equation (9)), while neglecting changes of B_x , which are substantial only within the “rippled ramp” region (roughly $-0.5 < x/(V_u/\Omega_u) < 0.5$). It is easily seen that the fluctuations of the total pressure in

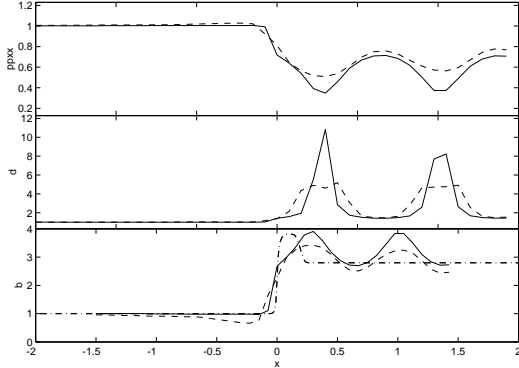


Figure 8. Comparison of the ion hydrodynamical variables for the shock with $M = 3.3$, $B_d/B_u = 2.8$, $\theta = 58^\circ$, $\beta_i = 0.05$, and $D = 0.1(c/\omega_{pi})$ [cf. Gedalin et al., 2000]. The top panel shows the total (ram and kinetic) pressure $nm_iV_x^2 + p_{xx}$, and the middle panel shows density. Variables for the one-dimensional shock are shown by solid lines; rippled shock ($L_y = 1.15(V_u/\Omega_u)$, $a_y = 0.2(c/\omega_{pi})$) variables are shown by dashed lines. The bottom panel shows the magnetic field calculated from the generalized pressure balance (equation (9)). The model magnetic field used for ion tracing is shown by the dash-dotted line.

the rippled case with $L_y = 1.15(V_u/\Omega_u)$ and $a_y = 0.2(c/\omega_{pi})$ (dashed line) are weaker than in the one-dimensional case (solid line). The density peaks in the rippled case are much lower than those in the one-dimensional case. The calculated magnetic field in the rippled case agrees better with the model magnetic field used for the numerical analysis (dash-dotted line). This example shows the ability of the rippling to smooth the downstream distribution and improve shock stability (better agreement with the model field means better stability in this case [Zilbersher et al., 1998; Gedalin et al., 2000]). Rippling always works toward smoothing downstream ion distributions but does not necessarily reduce the pressure. In this particular case the ion heating results in a pressure higher than it would be in the one-dimensional case, where it is insufficient to satisfy pressure balance condition. The density maxima, however, always decrease with rippling.

We must warn the reader that the above example does not allow us to conclude that rippling will *always* work toward stability improvement. It may well be that a particular set of parameters does not allow stable stationary shock at all and it has to be nonstationary. The above rippling parameters L_y and a_y were found after many unsuccessful tries, which emphasizes the necessity of fine tuning of the shock parameters. The only conclusion that can be drawn from the above example is that in some cases rippling scatters ions in such a way that the resulting shock structure is closer to the stable state than it would be if the shock were strictly one-dimensional. What exactly happens with this or that particular shock should be checked with the details of the shock structure taken into account. Unfortunately, direct testing of an observed shock, as it was done by Zilbersher et al. [1998] and Gedalin et al. [2000], does not seem possible, since we do not have the rippling parameters from existing one- or two-spacecraft measurements (unable at present to provide information about the three-dimensional structure of the shock front) and do not know what could determine the rippling scale and amplitude. It is possible that Cluster observations will change this situation. Another possibility is using the rippled shock structure found in 2-D and 3-D hybrid simulations and performing similar analyses of ion trajectories. This might be a subject of a separate study.

Yet another problem is the local (not averaged along the shock front) behavior of the hydrodynamical variables and possible implications for the shock stability. An answer to this question would require development of a theory of the rippled shock profile, which is well beyond the scope of the present paper.

We have seen that rippling in the y direction significantly affects the ion motion and ion distributions. This should be expected since the ion gyration occurs mainly in the x - y plane. For this reason we expect a much weaker effect from the rippling in the z direction. Figure 9 shows the ion trajectories for the case of rippling in the z direction, for the case when the rippling is stationary in the de Hoffman-Teller and the normal incidence frames. The first and third panels from the top correspond to the one-dimensional case. The rippling scale and amplitude are the same as in the previous case. One can see that rippling of this kind has only a minor effect on the ion trajectories.

4. Electrons

Tracing of electrons is similar to the tracing of ions except that there are upstream electrons whose velocity is upstream directed. These electrons should have come from the downstream region (only collisionless motion is considered), so in

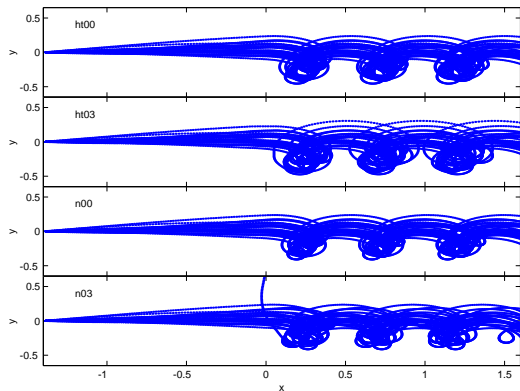


Figure 9. Ion trajectories in the case of rippling in the z -direction, for the case of the stationary rippling in two different frames. From top to bottom: no rippling in HT, rippling in HT, no rippling in NIF, and rippling in NIF. The rippling scale $L_z = 0.5(V_u/\Omega_u)$; amplitude $a_z = 0.3(c/\omega_{pi})$.

order to match the upstream electron distribution to the Maxwellian we have to trace these “leaking” electrons back to the past along their trajectories. For the presentation in this case we have chosen the dependence of v_z (which is essentially the electron velocity along the magnetic field) on the coordinate along the shock normal x in order to see whether such rippling can help to fill the gap (in v_z) in the collisionlessly formed downstream electron distribution. Figure 10 shows the electron

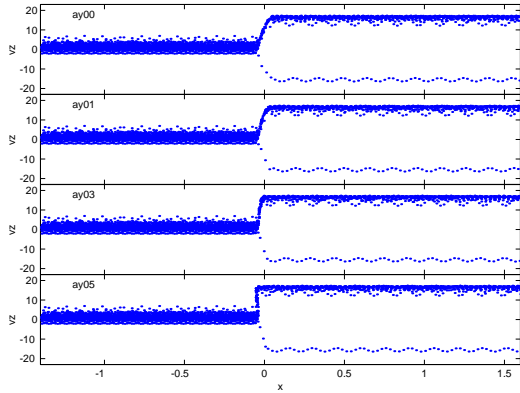


Figure 10. Electron trajectories for the case of the shock rippling in the y -direction with the rippling scale of $L_y = 0.5(V_u/\Omega_u)$ and various rippling amplitudes $a_y = 0.1(c/\omega_{pi})$, $0.3(c/\omega_{pi})$, and $0.5(c/\omega_{pi})$, increasing from top to bottom. The top panel corresponds to the one-dimensional case.

trajectories for the case of rippling in the y direction. The shock and rippling parameters are the same as in Figure 5. It is easily seen that electrons are almost insensitive to this kind of rippling.

Electrons are much more sensitive to rippling in the z direction, especially if it occurs in the normal incidence frame, as is seen from Figure 11 (same format as in Figure 9). In the last case the de Hoffman-Teller cross-shock potential becomes time dependent, and different electrons can acquire quite different energies. The gap in the downstream electron distribution becomes substantially filled. It should be noted, however, that electrons shown for the same coordinate x may in fact be in different y and z points, so the bottom panel is some kind of averaging over z .

5. Discussion and Conclusions

In the present paper we have studied the behavior of charged particles in a rippled shock front by numerically tracing ion and electron trajectories in the macroscopic stationary inhomogeneous magnetic and electric fields of the model shock profile. It should be emphasized that the study is not a (self-consistent) simulation where all inhomogeneity effects are mixed with the effects from possible nonstationarity of the shock front and waves and turbulence also. While self-consistent simulations allow us to see the effects observed in real shocks, they still do not allow us to distinguish consequences caused by different physical effects. Thus, though self-consistent simulations show the smoothing of downstream ion distribution, the interpretation of the mechanism of this smoothing (wave-particle interaction) is based on the analysis of the behavior

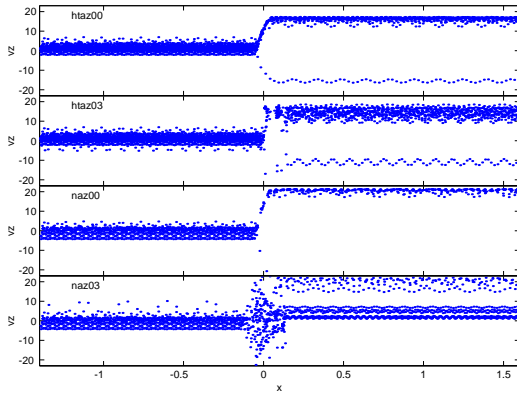


Figure 11. Electron trajectories in the shock rippled in the z -direction, for stationary rippling in two different frames. From top to bottom: no rippling in HT, rippling in HT, no rippling in NIF, and rippling in NIF. The rippling scale $L_z = 0.5(V_u/\Omega_u)$, and the rippling amplitude $a_z = 0.3(c/\omega_{pi})$.

of the wave spectrum together with the evolution of the ion distribution and not on the observation of the process of the interaction itself. It is at least very difficult to separate in self-consistent simulations the results of spatial inhomogeneity, large-scale nonstationarity, and turbulence, since all these mechanisms operate simultaneously. On the other hand, model analysis allows us to isolate particular effects by simply excluding others. In the present study we restricted the analysis to the consideration of the spatial inhomogeneity along the shock front only, which allowed to make definite conclusions about the effects of the shock rippling. We found that the rippling alone (without need in shock nonstationarity or wave-particle analysis) is capable of substantial smoothing of the downstream ion distributions. Such smoothing is rather efficient already at rippling scales of several ion inertial lengths with the rippling amplitude smaller than the shock width. The rippling efficiency depends on the direction of spatial inhomogeneity. Ions are mostly sensitive to the rippling in the noncoplanarity direction. This is because the source of ion gyration motion is the directed flow energy. Ions lose energy as they cross the shock and gyrate in the plane perpendicular to the magnetic field, which is the x - y plane in our case. Such y rippling makes the downstream ion distribution more smooth and diffuse, thus reducing the variations of the downstream ion pressure, which may improve the shock stability. These conclusions constitute certain predictions which, hopefully, can be tested with the beginning of the Cluster mission.

On the other hand, electrons are much more sensitive to rippling in the direction of the main magnetic field. This is because the source of energy for the electron acceleration and heating is the de Hoffman-Teller cross-shock electric potential, and energy gain may be much greater than the initial electron energy. The rippling may significantly affect the gap in the downstream electron distribution, yet it seems that the electron motion within the shock front has to be collisional to ensure more or less smooth electron distributions. It is not quite clear so far what could be responsible for the turbulent collisions. One possibility is a rapid development of the beam instability resulting in the efficient excitation of Langmuir waves and prompting further quasilinear diffusion [Bale *et al.*, 1998; Gedalin, 1999].

The issue worth discussing here is whether the rippled structure is nonstationary. It is clear that if the ripples propagate with (approximately) constant velocity along the shock front, there exists a frame in which the structure is approximately stationary. A good example is the above consideration of the rippling which is stationary in either the normal incidence or the de Hoffman-Teller frame and nonstationary in the other. This kind of frame-dependent nonstationarity should be considered in the same way as the above cases. Qualitative effects should be the same with possible quantitative differences (rippling scale and amplitude necessary for ion distribution smoothing), although the temporal dependence of the magnetic field in, for instance, the normal incidence frame may look complicated. The true nonstationarity, which cannot be eliminated by choosing an appropriate frame, requires a different approach. It is not quite clear which kind of nonstationarity is seen in numerical simulations. It is possible that sufficiently high Mach number shocks must be truly nonstationary. Effects of such nonstationarity of the shock profile at the ion timescales require separate study and are beyond the scope of the present paper.

Acknowledgments. Figures in the paper were prepared using Matlab.

The research was supported in part by Israel Science Foundation under grant 261/96-1. The author is grateful to the referees for stimulating comments. Janet G. Luhmann thanks Pierluigi Veltri and Marek Vandáš for their assistance in evaluating this paper.

References

- Bale, S.D., et al., Bipolar electrostatic structures in the shock transition region: Evidence of electron phase space holes, *Geophys. Res. Lett.*, 25, 2929, 1998.
- Balikhin, M., M. Gedalin, and A. Petrukovich, New mechanism for electron heating in shocks, *Phys. Rev. Lett.*, 70, 1259, 1993.
- Ball, L., and D. Galloway, Electron heating by the cross-shock electric potential, *J. Geophys. Res.*, 103, 17,455, 1998.
- Burgess, D., W.P. Wilkinson, and S.J. Schwartz, Ion distribution and thermalization at perpendicular and quasi-perpendicular supercritical collisionless shocks, *J. Geophys. Res.*, 94, 8783, 1989.
- Decker, R.B., Particle acceleration at shocks with surface ripples, *J. Geophys. Res.*, 95, 11,993, 1990.
- Decker, R.B., The role of magnetic loops in particle acceleration at nearly perpendicular shocks, *J. Geophys. Res.*, 98, 33, 1993.
- Feldman, W.C., Electron velocity distributions near collisionless shocks, in *Collisionless Shocks in the Heliosphere: Reviews of Current Research*, *Geophys. Monogr. Ser.*, vol. 35, edited by R.G. Stone and B.T. Tsurutani, pp. 195-205, AGU, Washington, D. C., 1985.
- Feldman, W.C., S.J. Bame, S.P. Gary, J.T. Gosling, D. McComas, M.F. Thomsen, G. Paschmann, N. Sckopke, M.M. Hoppe, and C.T. Russell, Electron heating within the Earth's bow shock, *Phys. Rev. Lett.*, 49, 199, 1982.
- Gedalin, M., Ion reflection at the shock front revisited, *J. Geophys. Res.*, 101, 4871, 1996a.
- Gedalin, M., Noncoplanar magnetic field in the collisionless shock front, *J. Geophys. Res.*, 101, 11,153, 1996b.
- Gedalin, M., Two-stream instability of electrons in the shock front, *Geophys. Res. Lett.*, 26, 1239, 1999.
- Gedalin, M., and E. Griv, Role of overshoots in the formation of the downstream distribution of adiabatic electrons, *J. Geophys. Res.*, 104, 14,821, 1999.
- Gedalin, M., K. Gedalin, M. Balikhin, and V.V. Krasnoselskikh, Demagnetization of electrons in the electromagnetic field structure, typical for oblique collisionless shock front, *J. Geophys. Res.*, 100, 9481, 1995a.
- Gedalin, M., K. Gedalin, M. Balikhin, V. Krasnoselskikh, and L.J.C. Woolliscroft, Demagnetization of electrons in inhomogeneous $\mathbf{E} \perp \mathbf{B}$: Implications for electron heating in shocks, *J. Geophys. Res.*, 100, 19,911, 1995b.
- Gedalin, M., J.A. Newbury, and C.T. Russell, Numerical analysis of collisionless particle motion in an observed supercritical shock front, *J. Geophys. Res.*, 105, 105, 2000.
- Goodrich, C.C., and J.D. Scudder, The adiabatic energy change of plasma electrons and the frame dependence of the cross shock potential at collisionless magnetosonic shock waves, *J. Geophys. Res.*, 89, 6654, 1984.
- Gosling, J.T., and A.E. Robson, Ion reflection, gyration, and dissipation at supercritical shocks, in *Collisionless Shocks in the Heliosphere: Reviews of Current Research*, *Geophys. Monogr. Ser.*, vol. 35, edited by R.G. Stone and B.T. Tsurutani, AGU, Washington, D. C., pp. 141-152, 1985.
- Gosling, J.T., and M.F. Thomsen, Specularly reflected ions, shock foot thicknesses, and shock velocity determinations in space, *J. Geophys. Res.*, 90, 9893, 1985.
- Hellinger, P., and A. Mangeney, Upstream whistlers generated by protons reflected from a quasiperpendicular shock, *J. Geophys. Res.*, 102, 9809, 1997.
- Hull, A.J., J.D. Scudder, L.A. Frank, W.R. Paterson, and M.G. Kivelson, Electron heating and phase space signatures at strong and weak quasi-perpendicular shocks, *J. Geophys. Res.*, 103, 2041, 1998.
- Jones, F.C., and D.C. Ellison, Noncoplanar magnetic fields, shock potentials, and ion deflection, *J. Geophys. Res.*, 92, 11,205, 1987.
- Jones, F.C., and D.C. Ellison, The plasma physics of shock acceleration, *Space Sci. Rev.*, 58, 259, 1991.
- Krasnosel'skikh, V., Nonlinear motions of a plasma across a magnetic field, *Sov. Phys. JETP, Engl. Transl.*, 62, 282, 1985.
- Krauss-Varban, D., and D. Burgess, Electron acceleration at nearly perpendicular collisionless shocks, 2, Reflection at curved shocks, *J. Geophys. Res.*, 96, 143, 1991.
- Krauss-Varban, D., F.G.E. Pantellini, and D. Burgess, Electron dynamics and whistler waves at quasi-perpendicular shocks, *Geophys. Res. Lett.*, 22, 2091, 1995.
- Lee, L.C., C.S. Wu, and X.W. Hu, Increase of ion kinetic temperature across a collisionless shock, 1, A new mechanism, *Geophys. Res. Lett.*, 13, 209, 1986.
- Lembege, B., and P. Savoini, Non-stationarity of a 2-D quasiperpendicular supercritical collisionless shock by self-reformation, *Phys. Fluids*, 4, 3533, 1992.
- Leroy, M.M., Structure of perpendicular shocks in collisionless plasma, *Phys. Fluids*, 26, 2742, 1983.
- Leroy, M.M., D. Winske, C.C. Goodrich, C.S. Wu, and K. Papadopoulos, The structure of perpendicular bow shocks, *J. Geophys. Res.*, 87, 5081, 1982.
- Livesey, W.A., C.T. Russell, and C.F. Kennel, A comparison of specularly reflected gyrating ion orbits with observed shock foot thicknesses, *J. Geophys. Res.*, 89, 6824, 1984.
- McKean, M.E., N. Omidi, and D. Krauss-Varban, Wave and ion evolution downstream of quasi-perpendicular bow shocks, *J. Geophys. Res.*, 100, 3427, 1995.
- Newbury, J.A., C.T. Russell, and M. Gedalin, The ramp widths of high-Mach-number, quasi-perpendicular collisionless shocks, *J. Geophys. Res.*, 103, 29,581, 1998.
- Savoini, P., and B. Lembege, Electron dynamics in two- and one-dimensional oblique supercritical collisionless magnetosonic shocks, *J. Geophys. Res.*, 99, 6609, 1994.
- Savoini, P., and B. Lembege, Full curvature effects of a collisionless shock, *Adv. Space Res.*, 24(1), 13, 1999.
- Schwartz, S.J., M.F. Thomsen, S.J. Bame, and J. Stansbury, Electron heating and the potential jump across fast mode shocks, *J. Geophys. Res.*, 93, 12,923, 1988.
- Scudder, J.D., A review of the physics of electron heating at collisionless shocks, *Adv. Space Res.*, 15(8/9), 181, 1995.
- Thomas, V.A., and D. Winske, Two dimensional hybrid simulation of a curved bow shock, *Geophys. Res. Lett.*, 17, 1247, 1990.
- Tidman, D.A., and N.A. Krall, Shock Waves in Collisionless Plasma, Wiley Interscience, New York, 1971.
- Vandas, M., Acceleration of electrons by a nearly perpendicular curved shock wave, 1, Zero shock thickness, *J. Geophys. Res.*, 100, 21,613, 1995a.
- Vandas, M., Acceleration of electrons by a nearly perpendicular curved shock wave, 2, Nonzero shock thickness, *J. Geophys. Res.*, 100, 23,499, 1995b.
- Veltri, P., and G. Zimbardo, Electron - whistler interaction at the Earth's bow shock, 1, Whistler instability, *J. Geophys. Res.*, 98, 13,325, 1993a.
- Veltri, P., and G. Zimbardo, Electron - whistler interaction at the Earth's bow shock, 2, Electron pitch angle diffusion, *J. Geophys. Res.*, 98, 13,335, 1993b.
- Veltri, P., A. Mangeney, and J.D. Scudder, Electron heating in quasi-perpendicular shocks: A Monte-Carlo simulation, *J. Geophys. Res.*, 95, 14,939, 1990.
- Veltri, P., A. Mangeney, and J.D. Scudder, Reversible electron heating vs. wave-particle interactions in quasi-perpendicular shocks, *Nuovo Cimento, Soc. Ital. Fis. C15*, 607, 1992.
- Wilkinson, W.P., and S.J. Schwartz, Parametric dependence of the density of specularly reflected ions at quasiperpendicular collisionless shocks, *Planet. Space Sci.*, 38, 419, 1990.
- Winske, D., and K.B. Quest, Magnetic field and density fluctuations at perpendicular supercritical collisionless shocks, *J. Geophys. Res.*, 93, 9681, 1988.
- Woods, L.C., On the structure of collisionless magnetoplasma shock waves at supercritical Alfvén Mach numbers, *J. Plasma Phys.*, 3, 435, 1969.
- Woods, L.C., On double structured, perpendicular, magneto-plasma shock waves, *J. Plasma Phys.*, 13, 289, 1971.
- Zilbershter, D., M. Gedalin, J.A. Newbury, and C.T. Russell, Direct numerical testing of stationary shock model with low Mach number shock observations, *J. Geophys. Res.*, 103, 26,775, 1998.